11. CO oxidation over O/Au(110)-(1×2)

In the preceding chapters, we studied the of the adsorption of the CO oxidation reactants, CO and O_2, the product CO_2, and the generation of an reactive intermediate, chemisorbed atomic oxygen. Thereby we obtained information which is essential for the qualitative and quantitative understanding of the CO oxidation reaction. We now proceeded as follows: first, we performed reactive thermal desorption measurements (RTDM) in order to obtain qualitative information about the temperature dependence of the overall reaction rate. Second, we studied the time dependence of the CO_2 desorption rate under isothermal conditions for different initial oxygen coverages. Finally, we investigated the time-dependence of the rate for various fixed temperatures at constant initial oxygen coverage. The latter experiments allow, within the framework of an appropriate model, the determination of the apparent and of the true activation energy of the surface reaction. Additional UPS investigations of the oxidation process allow insight into the reactivity below the CO_2 desorption temperature.

11.1. The reactivity of chemisorbed oxygen towards CO - reactive thermal desorption measurements (RTDM)

First, we were interested in the temperature-dependence of the oxygen reactivity in a stationary CO atmosphere (p_{CO} = 1×10^{-6} mbar). In the respective experiment, the temperature of the oxygen-precovered sample was swept with a heating rate of 2.35 K/s and the evolution of the oxidation product CO_2 was measured by means of mass spectrometry. The resulting curve, corresponding to an initial coverage of 1.3 ML chemisorbed oxygen, is plotted in Fig. 11.1a. For comparison, we show a CO TD spectrum (1.0 ML CO) from clean Au(110)-(1×2) (Fig. 11.1b) and a CO_2 TD spectrum (1.0 ML CO_2) from the same surface precovered with 1.3 ML chemisorbed oxygen (Fig. 11.1c).

Fig. 11.1a reveals that chemisorbed oxygen reacts vigorously with CO well below room temperature. The curve shows three maxima around 67 K, 105 K, and 175 K, which can easily be understood by comparison with Figs. 11.1b and c. According to the latter, CO_2 desorbs from the oxygen-precovered gold surface only above 90 K[1]. We conclude that the peak ρ_2 around 105 K in Fig. 11.1a is due to the desorption of CO_2 formed below and right at 105 K. The remarkable CO_2 peak ρ_1 around 67 K indicates that molecules excited by the reaction energy may surmount the activation barrier for desorption below the thermal desorption temperature. Above 135 K, the equilibrium concentration of CO_2 on the surface is stationary and very low and, therefore, the desorption rate equals the reaction rate. The latter increases between 135 K and 175 K, because the rate constant grows exponentially with temperature. Simultaneously, the equilibrium surface concentration of CO decreases. This leads to a drop in the reaction rate beyond 175 K

[1] A detailed study of CO_2 adsorption on the oxygen-precovered gold surface can be found in Section 10.5.

(maximum ρ_3). The corresponding CO TDS in Fig. 11.1b indicates that the CO concentration becomes very low around this temperature. (Adsorption isotherms of the system CO/Au(110)-(1×2) as displayed in Fig. 8.14 show that the equilibrium CO coverage is $\Theta_{CO} = 0.1$ ML at 175 K for a CO pressure of 1×10^{-6} mbar.) Additionally, the reaction rate is further reduced by a decrease of the oxygen coverage.

By comparison of the CO_2 desorption flux with the flux of CO onto the surface (as calculated by the collision flux or Hertz-Knudsen equation, Eq. 4.32), we can determine the CO/CO_2 conversion probability, P_{CO/CO_2}, which can be interpreted as the product of CO sticking and reaction probability. At the rate maximum ρ_3, which corresponds to an oxygen coverage of 0.45 ML and a temperature of 175 K, we found a value of $P_{CO/CO_2} = 0.07$.

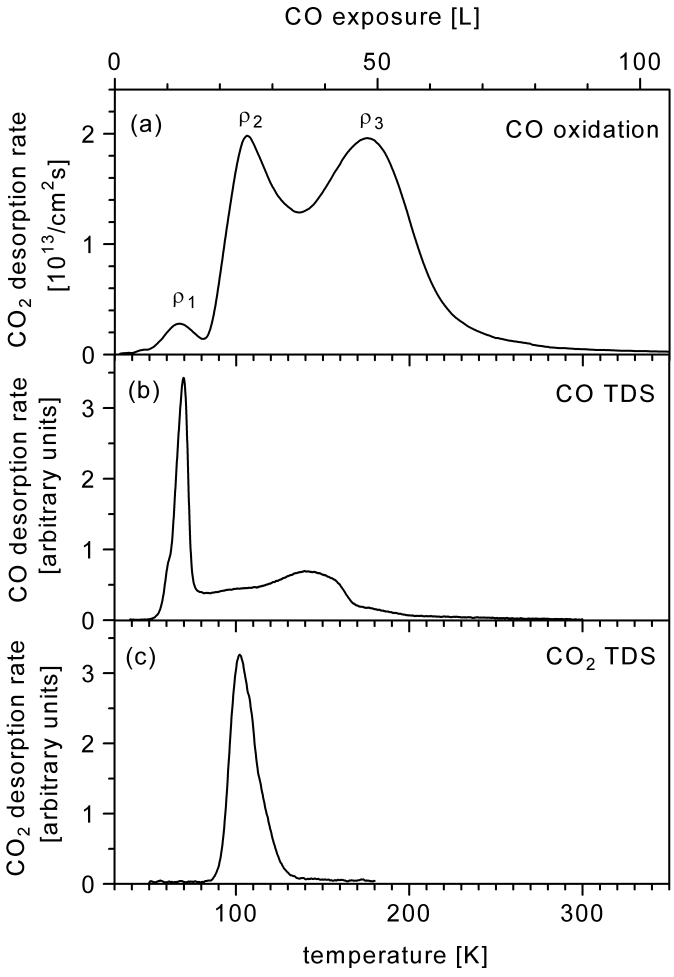

Fig. 11.1: (a) CO oxidation over O/Au(110)-(1×2) at an initial O coverage of 1.3 ML and a CO pressure of 1×10^{-6} mbar. Desorption rate of the reaction product CO_2 as a function of temperature. Heating and CO flux were started simultaneously. The upper abscissa, showing the total CO exposure, applies only to Fig. 11.1a. TD spectra of (b) CO/Au (inital CO coverage 1.0 ML) and (c) CO_2/O/Au (initial CO_2 coverage 1.0 ML, O coverage 1.3 ML). The heating rate was always 2.35 K/s. Detected masses: m/z = 28 (CO^+), m/z = 44 (CO_2^+).

11.2. Influence of the initial oxygen coverage on the reactivity

In a second type of experiment, we measured the CO_2 desorption rate as a function of time for various initial oxygen coverages at a constant temperature of 200 K and a CO pressure of 1×10^{-6} mbar. This temperature is well above the CO_2 desorption temperature to ensure that desorption and reaction rates are equal. The resulting curves are displayed in Fig. 11.2 and reveal that the reaction rate is not a unique function of the *instantaneous* oxygen coverage, but depends also upon the *initial* coverage at any time. Higher oxygen coverages obviously inhibit the reaction with CO. This phenomenon is reminicent of the auto-inhibition of the oxygen desorption reaction, which could successfully explained with the formation of oxygen islands as extensively discussed in Chaper 6. These islands are likely to react with CO only at their perimeters, which means that the effective coverage (which enters the respective rate equations) is smaller than the total coverage. The curve corresponding to an initial coverage of 1.9 ML even has a maximum which occurs after an induction period of ≈ 50 s. The following explanation is most likely: The initial aggregates are large and compact; the effective coverage is small. As the reaction proceeds, the islands erode and, thus, the effective coverage increases, which in turn leads to an increase of the reaction rate despite decreasing total coverage.

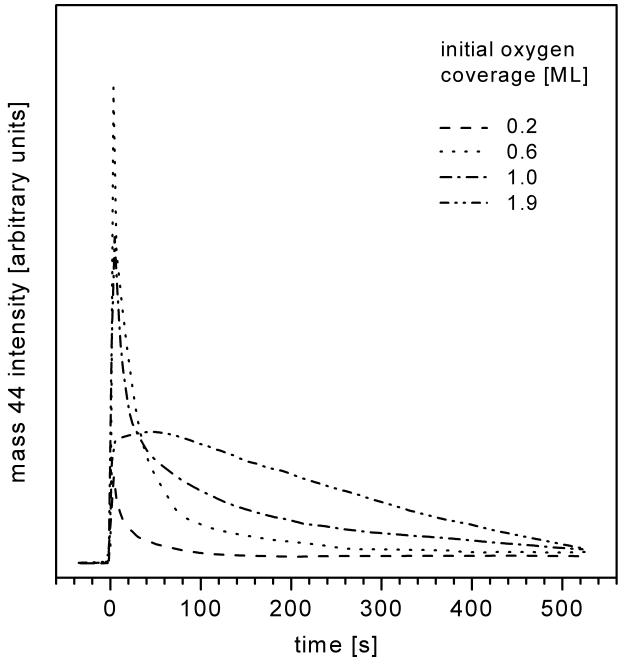

Fig. 11.2: CO oxidation over O/Au(110)-(1×2) at 200 K. CO_2 desorption rate as a function of time for several initial oxygen coverages $\Theta_0(O_{ad})$ as indicated. At t = 0, the CO pressure was raised to 1×10^{-6} mbar. Detected mass: m/z = 44 (CO_2^+). The chemisorbed oxygen phase was prepared by electron bombardment of physisorbed O_2 and subsequent annealing at 450 K.

Oxygen TDS (mass 32) taken after exposure of the oxygen phase to ≈ 700 L CO at 200 K proved the complete removal of both oxygen species β_1 and β_2, indicating a sufficient accessibility for the CO molecules to react. Since the oxygen atoms are not mobile in the bulk on the time-scale of our experiment and at the given temperature, they must be located within the first atomic layers for both β_1 and β_2. Obviously, a bulk oxygen species is not produced by electron bombardment of physisorbed dioxygen.

11.3. Kinetics of the CO oxidation reaction

Fig. 11.3 displays the CO_2 desorption rate, R_{CO_2}, as a function of time for various fixed temperatures between 60 K and 400 K. In all measurements, the following procedure was applied: a chemisorbed atomic oxygen phase of 0.45 ML was prepared at 30 K by electron bombardment of physisorbed O_2 as described in Chapter 5. To ensure a uniform oxygen phase in all experiments the sample was heated to 450 K (see further below for a justification of this annealing step). Then, the sample temperature was set to a constant value and the CO pressure was (almost) instantaneously increased to 1×10^{-6} mbar. The resulting CO_2 desorption flux was measured with a mass spectrometer. All curves in Fig. 11.3 exhibit an approximately exponential decrease of the CO_2 desorption rate.

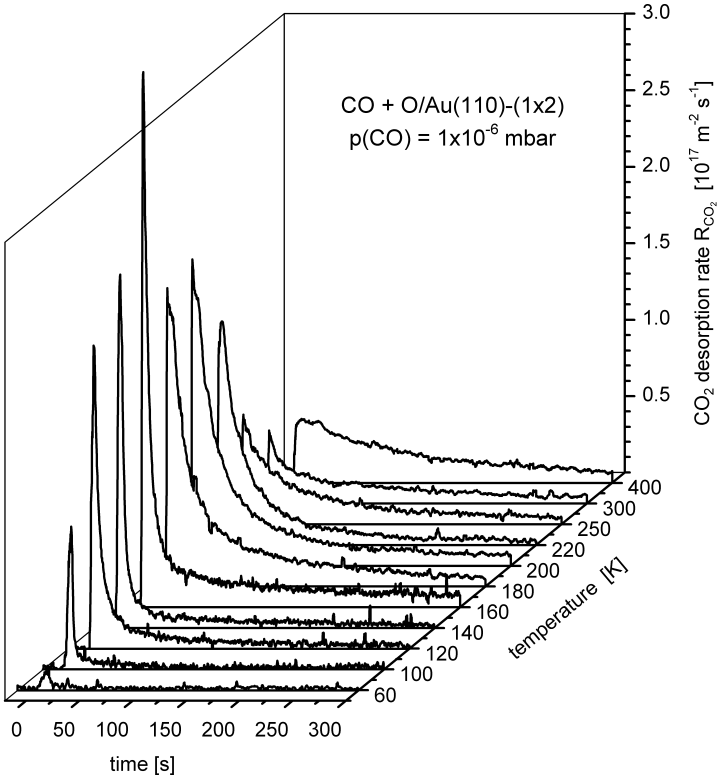

Fig. 11.3: CO oxidation over O/Au(110)-(1×2). CO_2 desorption rate as a function of time for temperatures between 60 K and 400 K. Detected mass: m/z = 44 (CO_2^+).

First, we consider only the initial rates in a qualitative manner: In the low-temperature range between 60 K and 160 K, the rate increases with temperature, which is certainly due to the increase of the reaction rate constant k_r with temperature. However, temperatures above 180 K lead to a decrease of the reaction rate with increasing temperature, which implies a negative apparent activation energy. The maximum rate at 160 K agrees with the maximum ρ_3 in Fig. 11.1. The most likely cause is a decrease of the CO equilibrium coverage with increasing temperature, which is obviously not compensated by the increase of the reaction rate. The behaviour in the high-temperature range strongly suggests a Langmuir-Hinshelwood type of reaction, since it cannot be understood without assuming that only adsorbed CO reacts with the chemisorbed oxygen.

Assuming a Langmuir-Hinshelwood reaction, we can derive a mechanism that allows a quantitative analysis and the determination of the true activation energy of the surface reaction. The following mechanism can be proposed:

$$O_2\,(g) \underset{k_{d,O2}}{\overset{k_{a,O2}}{\rightleftharpoons}} O_2\,(ad) \qquad \text{(Eq. 11.1)}$$

$$O_2\,(ad) \underset{k_{rec,O}}{\overset{k_{diss,O2}}{\rightleftharpoons}} 2O\,(ad) \qquad \text{(Eq. 11.2)}$$

$$CO\,(g) \underset{k_{d,CO}}{\overset{k_{a,CO}}{\rightleftharpoons}} CO\,(ad) \qquad \text{(Eq. 11.3)}$$

$$CO\,(ad) + O\,(ad) \xrightarrow{k_r} CO_2\,(ad) \qquad \text{(Eq. 11.4)}$$

$$CO_2\,(ad) \xrightarrow{k_{d,CO2}} CO_2\,(g) \qquad \text{(Eq. 11.5)}$$

We exclude Eqs. 11.1 and 11.2 from our consideration, since O(ad) is here not produced by the spontaneous process described by Eqs. 11.1 and 11.2.

In the following, we derive an expression for the CO_2 desorption rate $R_{CO_2} = dN_{CO_2}/(Adt)$.

$$R_{CO_2} = k_{d,CO_2}\Theta_{CO_2} = -\frac{d\Theta_O}{dt} \quad . \qquad \text{(Eq. 11.6)}$$

For temperatures above the CO_2 desorption temperature on oxygen-precovered gold, ≈ 120 K, the CO_2 equilibrium coverage, Θ_{CO_2}, is very low and (quasi)-stationary. Thus, we can apply the following steady-state condition to Θ_{CO_2}:

$$\frac{d\Theta_{CO_2}}{dt} = -k_{d,CO_2}\Theta_{CO_2} + k_r\Theta_{CO}\Theta_O \cong 0 \quad . \qquad \text{(Eq. 11.7)}$$

Eliminating Θ_{CO_2} from Eqs. 11.6 and 11.7 yields:

$$R_{CO_2} = k_r \Theta_{CO} \Theta_O = -\frac{d\Theta_O}{dt} \quad . \qquad \text{(Eq. 11.8)}$$

With an excess of CO in the gas phase, we can now also eliminate Θ_{CO} if we assume that the CO adsorption/desorption equilibrium is only minimally disturbed by the oxidation reaction, which removes CO from the equilibrium. We demonstrate that this assumption is reasonable for not too small CO sticking coefficients: At the given CO pressure and gas temperature, the CO flux onto the surface amounts to 2.9×10^{18} $m^{-2}s^{-1}$. For comparison, the maximum intensity seen in Fig. 11.3 (160 K curve, t = 0) is equivalent to 3.4×10^{17} $m^{-2}s^{-1}$, i.e., ≈ 10% or less of the impinging CO molecules react with oxygen atoms to CO_2. Thus, the approximate CO coverage is given by the Langmuir isotherm, at least for a small coverage range in which the isosteric heat is approximately constant:

$$K \equiv \frac{k_{a,CO}}{k_{d,CO}} = \frac{\Theta_{CO}}{p_{CO}(1-\Theta_{CO})} \approx \frac{\Theta_{CO}}{p_{CO}} \quad \text{for } \Theta_{CO} << 1 \qquad \text{(Eq. 11.9)}$$

At the given CO pressure and temperatures above 160 K, the equilibrium CO coverage is low, e.g. ≈ 0.05 ML at 180 K and p(CO) = 10^{-6} mbar (see Chapter 8, Fig. 8.14).Thus, we can neglect Θ_{CO} in the denominator on the right hand side of Eq. 11.9.

Combining Eqs. 11.8 and 11.9 (simplified) under elimination of Θ_{CO} yields:

$$R_{CO_2} = -\frac{d\Theta_O}{dt} = \frac{k_{a,CO} k_r}{k_{d,CO}} p_{CO} \Theta_O \equiv k_{exp} \Theta_O \qquad \text{Eq. 11.10}$$

with the empirical rate constant k_{exp}. Thus, the mechanism in Eqs. 11.1-5 in combination with our additional assumptions predicts a pseudo-first order reaction. Applying the Arrhenius equation to the rate constants k_i in Eq. 11.10 leads to te following expression for k_{exp}:

$$k_{exp} = k_{a,CO}\, p_{CO}\, \frac{\nu_r}{\nu_{d,CO}}\, e^{-(E_r - E_{d,CO})/RT} \qquad \text{Eq. 11.11}$$

with the CO desorption energy E_d, the activation energy of the oxidation step (Eq. 11.4) E_r, and the respective frequency factors $\nu_{d,CO}$ and ν_r. Eq. 11.11 shows that the apparent

activation energy of the overall reaction, $E_r - E_{d,CO}$, can be obtained from the slope of a plot of ln k_{exp} vs. 1/T.

In order to evaluate $k_{exp}(T)$ from the curves in Fig. 11.3, we integrate the rate equation Eq. 11.10 and obtain

$$\ln \frac{\Theta_O}{\Theta_{O,t=0}} = -k_{exp} t \qquad \text{Eq. 11.12}$$

with the initial oxygen coverage $\Theta_{O,t=0}$.

With Eq. 11.12 we can replace Θ_O in Eq. 11.11:

$$R_{CO_2} = -\frac{d\Theta_O}{dt} \equiv k_{exp}\ \Theta_{O,t=0}\ e^{-k_{exp}t} \ . \qquad \text{Eq. 11.13}$$

Thus, k_{exp} is given by:

$$k_{exp} = -\frac{d \ln R_{CO_2}}{dt} \ . \qquad \text{Eq. 11.14}$$

According to Eqs. 11.11 and 11.14, the slope of a plot of $\ln\left(-\frac{d \ln R_{CO_2}}{dt}\right)$ vs. 1/T is $-(E_r - E_{d,CO})/R$, i.e., it is equal to the apparent overall reaction activation energy. Such a plot for temperatures between 200 K and 400 K is shown in Fig. 11.4 and yields $(E_r - E_{d,CO}) = (-1.8 \pm 0.9)$ kJ/mol. This negative value is in agreement with the obvious decrease of the rate with increasing temperature above ≈ 160 K in Figs. 11.1 and 11.3. Determination of the true activation energy, E_r, requires knowledge of the CO desorption energy, $E_{d,CO}$. In Section 8.5, we evaluated the isosteric heat of CO adsorption at zero coverage, $Q_{st} = (59 \pm 2)$ kJ/mol, which is, for a mobile adsorbate layer, equal to the CO binding energy. Since CO adsorption is non-activated (as sown in Section 8.5), we can identify the binding energy with the desorption energy and thus obtain a value of $E_r = (57 \pm 3)$ kJ/mol for the true activation energy. This value is higher than the activation energy for the gas phase reaction between CO and oxygen atoms, which is 15 kJ/mol [Cl62]. The difference between E_r and the gas phase value can be interpreted as the energy expense for the rehybridization of the adsorbate-substrate bonds of CO and oxygen in the activated complex.

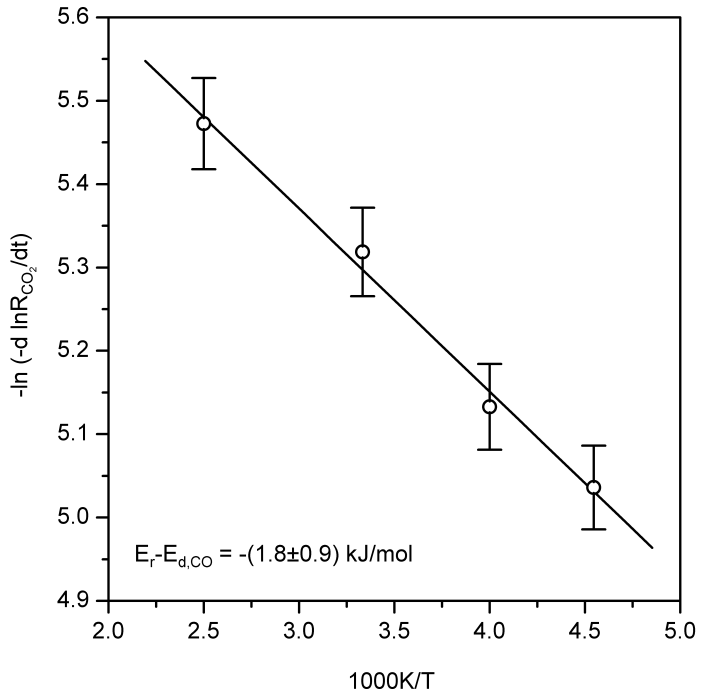

Fig. 11.4: Plot of $\ln\left(-\mathrm{d}\ln R_{CO_2}/\mathrm{dt}\right)$ vs. 1/T. The gradient of the linear fit is the apparent overall reaction activation energy - $(E_r - E_{d,CO})/R$.

A closer inspection of the curves in Fig. 11.3 reveals that the plots of $\ln R_{CO_2}$ vs. 1/T actually deviate from linearity, especially in the low-temperature range below 180 K (Fig. 11.5). In the following, we consider several possible causes which partly arise from the simplifications we applied for deriving the Eqs. 11.11 and 11.14, and critically discuss further implicite assumptions of our model.

(a) We assumed that $\Theta_{CO} \propto p_{CO}$ (Eq. 11.10), which is only valid for small Θ_{CO}. Furthermore, we supposed that the equilibrium between CO(g) and CO(ad) is not disturbed by the reaction of CO with chemisorbed oxygen. Now we lift these limitations and demonstrate that the complete solution contains an additional term in which Θ_O is proportional to t. We assume steady-state conditions for CO(ad) and obtain:

$$\frac{\mathrm{d}\Theta_{CO}}{\mathrm{dt}} = k_{a,CO} p_{CO}(1-\Theta_{CO}) - k_{d,CO}\Theta_{CO} - k_r \Theta_{CO}\Theta_O = 0\,. \qquad \text{(Eq. 11.15)}$$

Herein, we still assume a constant $k_{d,CO}$, which requires a coverage-independent CO desorption energy, and a constant $k_{a,CO}$, which implies that the CO sticking coefficient is independent of temperature (see below).

With Eq. 11.15, we eliminate Θ_{CO} from Eq. 11.8 and obtain instead of Eq. 11.10:

$$R_{CO_2} = -\frac{d\Theta_O}{dt} = \frac{k_{a,CO}\, k_r\, p_{CO}}{k_{a,CO}\, p_{CO} + k_{d,CO} + k_r\, \Theta_O}\Theta_O \equiv k_{exp}\Theta_O \qquad \text{(Eq. 11.16)}$$

Eq. 11.16 reveals that the experimental rate constant, k_{exp}, is actually not independent of the oxygen coverage Θ_O. Integration yields:

$$\ln\frac{\Theta_O}{\Theta_{O,t=0}} + \frac{k_r}{k_{a,CO} + k_{d,CO}}\left(\Theta_O - \Theta_{O,t=0}\right) = -\frac{k_r\, k_{a,CO}\, p_{CO}}{k_{a,CO}\, p_{CO} + k_{d,CO}}\, t\ . \qquad \text{(Eq. 11.17)}$$

The second term on the left hand side of Eq. 11.17 leads to a deviation from the first-order kinetics. The occurence of $k_{a,CO} + k_{d,CO}$ in the denominator indicates that these deviations increase when the CO adsorption and desorption rates are small, i.e., at low temperatures and low CO pressures.

(b) The CO sticking coefficient S_{CO} and the desorption rate constant $k_{d,CO}$ may depend on the oxygen coverage Θ_O, which decreases during the reaction. Especially $k_{d,CO}$ is likely to vary with Θ_O. In the case of CO_2/O/Au we found a considerable increase of the desorption activation energy due to the oxygen-precoverage which led to a shift of the CO_2 desorption peak from 91 K to 118 K (see Section 10.5 and Fig. 10.11). We are also able to demonstrate the effect of preadsorbed oxygen on the CO adsorption directly: Fig. 11.6 displays a CO TDS from oxygen-covered gold with $\Theta_O \approx 0.3$ ML. The spectrum exhibits an additional peak around 185 K, which corresponds to an increase of the desorption energy of ≈ 8 kJ/mol relative to the ε-CO peak on the clean surface. Still, a quantitative consideration of this effect is difficult because it is unclear whether or not the O-covered surface actually provides adsorption sites with higher desorption energy. Desorption in this temperature range is also observed on the clean surface (with much lower intensity, see Section 8.1), and it is possible that only the number of the sites with high desorption energy increases, not their energy. Isosteric heat measurements, as described for CO adsorption on clean gold (Section 8.5), would provide reliable binding energies as a function of coverage, but these measurements are impossible to perform because of the reaction between CO and O(ad).

(c) The Langmuir isotherm, which was used in Eqs. 11.9 and 11.15, is only valid for very small CO coverages (i.e., at elevated temperatures), because the isosteric heat of CO is strongly coverage-dependent (see Fig. 8.16) and, thus, $k_{d,CO}$ is a function of the CO coverage, $k_{d,CO} = k_{d,CO}(\Theta_{CO})$. Furthermore, $k_{a,CO}$ contains the CO sticking coefficient S_{CO}. If S_{CO} is a function of temperature, the temperature dependence of k_{exp} is not restricted to the exponential term in Eq. 11.11, which was implicitly assumed when we derived the apparent activation energy from the plot in Fig. 11.4.

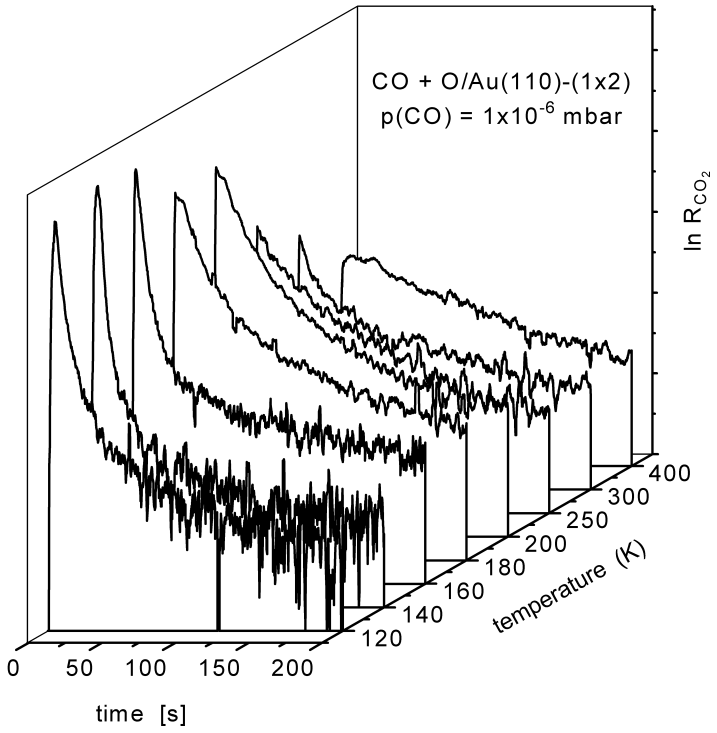

Fig. 11.5: Semi-logarithmic plot of several curves from Fig. 11.3. See the text for the details.

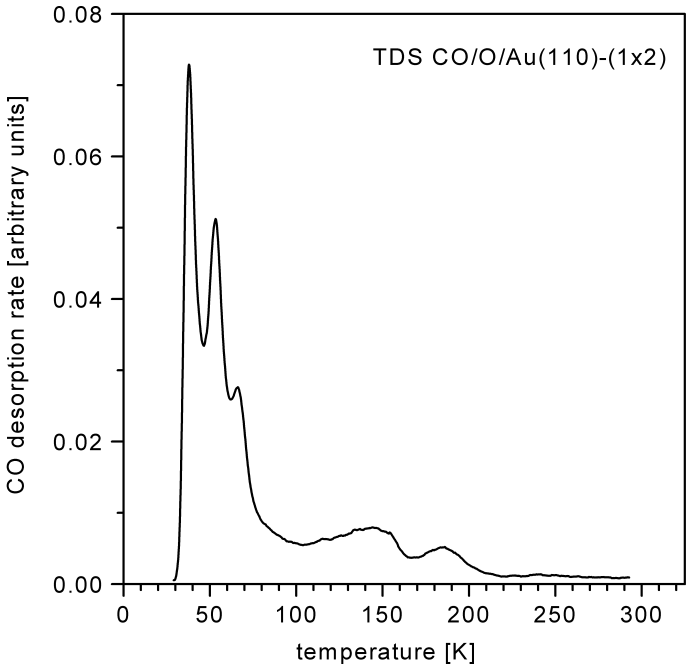

Fig. 11.6: CO-TDS from the oxygen-precovered gold surface ($\Theta_O \approx 0.3$ ML). CO dosage 3.2 L, heating rate 2.35 K/s, detected mass m/z = 28. Compare with Figs. 8.1 and 8.6.

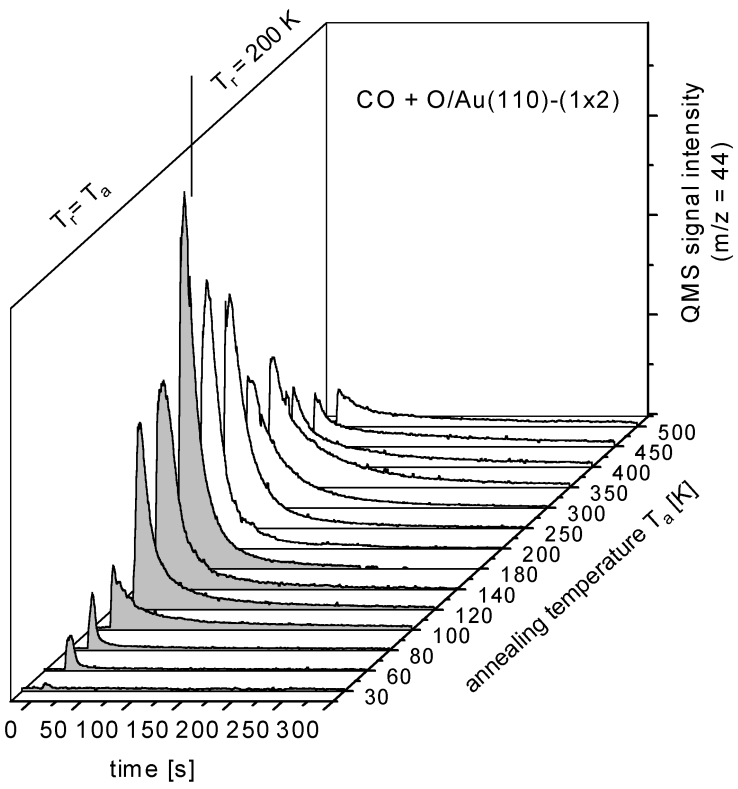

Fig. 11.7: CO oxidation over O/Au(110)-(1×2). CO_2 desorption rate as a function of time. Chemisorbed oxygen (with an initial coverage of 1.0 ML) was prepared by electron irradiation of physisorbed O_2 at 30 K. The chemisorbed oxygen phase was annealed at the indicated temperatures T_a between 30 K and 500 K. The reaction temperature T_r for the CO oxidation was 200 K for $T_a \geq 200$ K and $T_r = T_a$ for $T_a < 200$ K. The increase of the rate in the range between 30 K and 180 K, which is less informative because two parameters are simultaneously varied, is probably mainly due the increase of the reaction temperature as discussed above. See the text for further details.

(d) The oxygen phase may be less homogeneous than the oxygen TDS in Chapter 6 suggests, leading to a variety of oxygen adsorption states with different reactivity towards CO. This idea is supported by the UPS measurements in Section 11.4 and by the apparent contradiction between the relatively high activation energy of $E_r = (57 \pm 3)$ kJ/mol and the fact that the reaction occurs already below 100 K. This point will be discussed in Section 11.4.

VARIATION OF THE ANNEALING TEMPERATURE – In a further type of experiments, we varied the temperature at which the oxygen phase was annealed after the preparation (by electron bombardment of physisorbed O_2 at 30 K) and prior to the reaction, performed at constant CO pressure (1×10^{-6} mbar) and temperature. The resulting R_{CO2} vs. time curves are shown in Fig. 11.7. We distinguish between two regions with different regimes for the reaction temperature. If the sample was annealed at and below 180 K, we performed the CO oxidation at the same temperature as the annealing (gray filling in Fig. 11.6). Otherwise the curves were taken at a sample temperature of 200 K

(white filling). In the high-temperature range between 180 K and 500 K we observe that the initial rate decreases despite the constant reaction temperature. The chemisorbed oxygen is apparently deactivated by heating to elevated temperatures. We say apparently, because it is similarly likely that a decrease of the CO equilibrium concentration is responsible for this effect. Annealing reduces the number of defect sites which are possibly formed in the process of the electron stimulated dissociation of physisorbed oxygen. It was shown in Section 8.1 that the desorption energy of CO is higher on a gold surface with a large defect concentration than on an annealed surface (cf. Fig. 8.6). Thus, the reduced defect concentration after annealing leads to a smaller CO equilibrium concentration on the surface and thus to a lower reaction rate. The oxygen reactivity may also decrease by the annealing process, because it can lead to the formation of islands or to the growth of larger islands on the expense of smaller ones. It is likely that the oxygen atoms which are condensed in islands possess a reduced reactivity (see Section 11.2). As an illustration, we show in Fig. 11.8 RTDM curves for different annealing temperatures of the chemisorbed oxygen phase. Annealing obviously reduces (but not completely suppresses) the intensity of the low-temperature ρ_2 peak, whereas ρ_3 remains unaffected or even grows.

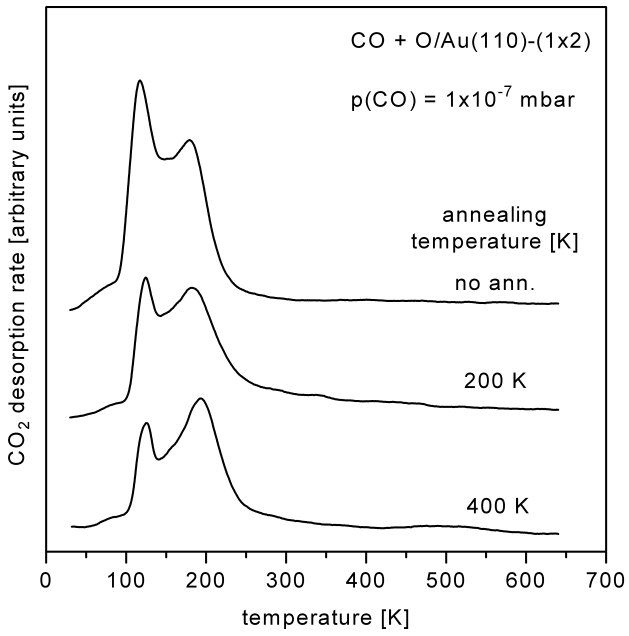

Fig. 11.8: CO oxidation over O/Au(110)-(1×2) at an initial O coverage of 1.0 ML and a CO pressure of 1×10^{-7} mbar. The chemisorbed oxygen phases were annealed at the indicated temperatures prior to the CO oxidation. Heating rate 2.35 K/s, detected mass m/z = 44 (CO_2^+). The chemisorbed oxygen is not completely consumed by the CO oxidation under the reaction conditions, as a simultaneously recorded oxygen TDS reveals.

11.4. UPS investigation of the CO oxidation

The RTDM curve displayed Fig. 11.1 indicates that CO_2 formation occurs already at very low temperatures below 100 K. This fact is in apparent contradiction to the relatively high value of the reaction activation energy E_r as evaluated in Section 11.3, which implies that measurable rates occur only above 150 K. We conclude that several oxygen species with different reactivity are initially present and that the annealing at 450 K prior to the CO oxidation leaves only that with the low reactivity. In order to verify this hypothesis we performed the following temperature-dependent UPS experiments.

We prepared 1.0 ML chemisorbed oxygen by electron irradiation of physisorbed O_2 as described in Chapter 5 and heated the sample to 350 K. After cooling to 30 K, we adsorbed 3.0 L (≈ 1.6 ML) CO, increased stepwise the temperature and measured a UP spectrum after each T-step. Fig. 11.9 displays the resulting spectra.

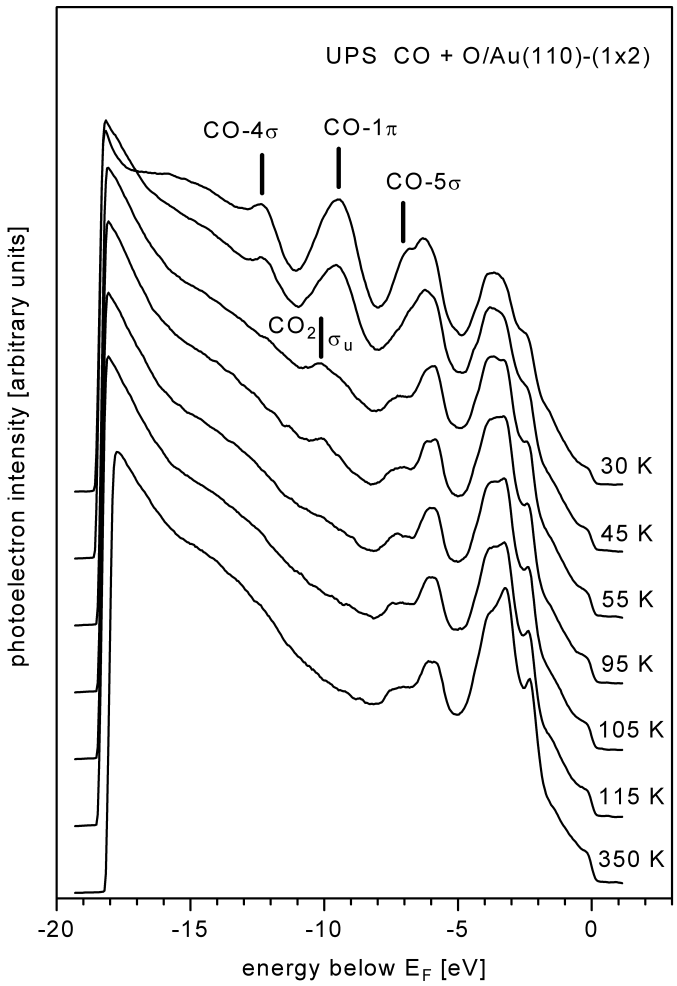

Fig. 11.9: UP spectra (hν = 24 eV) of 1.6 ML CO adsorbed on O/Au(110)-(1×2). The sample temperature was stepwise increased. Initial oxygen coverage 1.0 ML. M polarization, normal emission, sample bias -10 V.

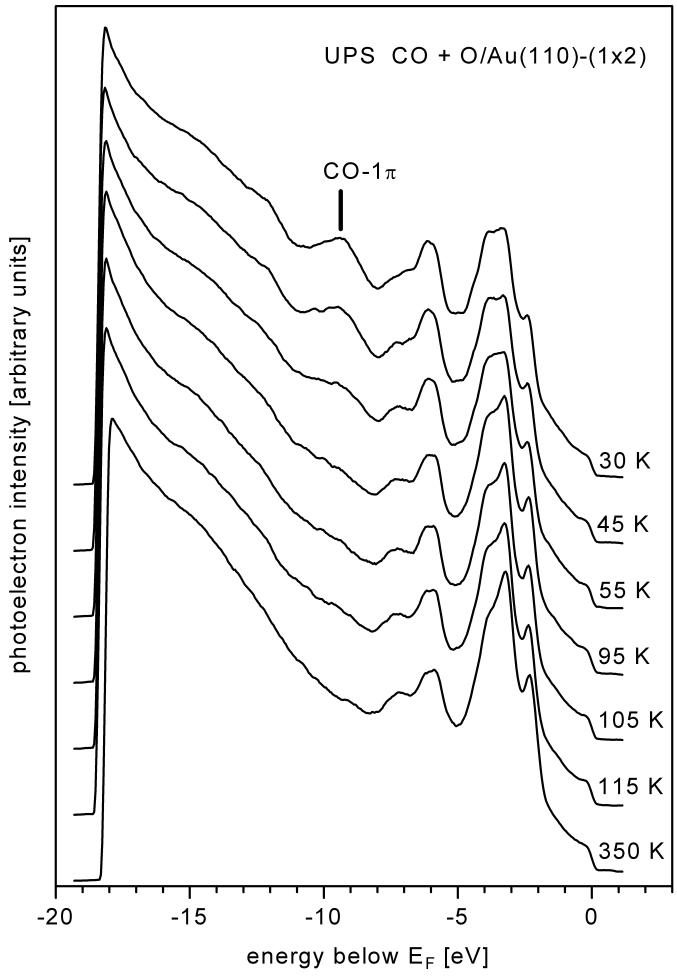

Fig. 11.10: UP spectra ($h\nu = 24$ eV) of 0.8 ML CO adsorbed on O/Au(110)-(1×2) for increasing temperatures. The oxygen phase was previously treated with CO, which removed the oxygen species with the higher reactivity. Oxygen coverage at the beginning of the experiment ≈ 0.7 ML. M polarization, normal emission, sample bias -10 V.

The spectrum at 30 K shows the signals of physisorbed CO, which are shifted by ≈ 1 eV (the amount of the oxygen-induced work function change) towards lower binding energies relative to CO on the clean surface. (The reason for this shift was extensively discussed in Section 5.2.3 on the example of O_2/O/Au(110)-(1×2).) Heating to 45 K leads to shoulder around -10.6 eV, which can be attributed to the CO_2 σ_u and π_u levels and which undergo the same $\Delta\varphi$-induced shift relative to CO_2 on clean gold as observed for the CO levels. Thus, we can state that the CO oxidation occurs already below 45 K. Above 55 K, the spectra are dominated by the intense double peak of the CO_2 levels σ_u and π_u with a maximum at -10.2 eV. The signals of remaining CO are hardly visible because of the strong overlap with the CO_2 signals. These signals vanish between 95 K and 115 K, i.e., in the temperature range where the thermal desorption of CO_2 on O/Au(110)-(1×2) occurred (see Section 10.5 and Fig. 10.11). Above 115 K, no CO

induced signal can be seen in the spectra, indicating that all CO molecules did either desorb or react with oxygen below this temperature.

After this experiment, the sample was heated to 350 K and again cooled to 30 K. The work function change relative to the clean surface indicated a residual oxygen coverage of ≈ 0.7 ML. Now we adsorbed again CO, this time 1.5 L (≈ 0.8 ML) and performed the same temperature-dependent experiment as above. The resulting UP spectra are displayed in Fig. 11.10. Visible is one peak around -9.3 eV, which can be assigned to the 1π level of physisorbed CO if a peak shift towards lower binding energies (relative to CO on clean gold) by the amount of the oxygen-induced work function change (0.8 eV) is taken into account. This peak diminished upon heating due to the gradual thermal desorption of CO. No intermediate CO_2 signals appeared. We conclude that the oxygen species which is reactive below the CO_2 desorption temperature was completely consumed already in the first cycle and that only less reactive oxygen is left. Only the latter can be characterized by the reaction activation energy of 57 kJ/mol which was evaluted in the preceding section.

11.5. Comparison with literature data

Numerous studies have been devoted to the CO oxidation as the simplest oxidation reaction that can be investigated on metal surfaces. In the following, we confine ourself to comparing our data with relevant CO oxidation studies on Cu, Ag, and Au surfaces. Carbon monoxide is readily oxidized on all coinage metal surfaces precovered with chemisorbed oxygen. The apparent activation energies (E_r-$E_{des,CO}$) are in general small, indicating that CO desorption energy $E_{des,CO}$ and reaction activation energy E_r are not very different for all three metals.

On the (110)- and (111)-surfaces of copper, the CO oxidation rate was reported to be proportional to the CO pressure. For the apparent activation energy values between 20 and 30 kJ/mol were found. An exeptional high value was reported for Cu(100) (see Table 11.1 for the references). The reaction kinetics becomes complicated at high oxygen loadings, when subsurface oxygen is formed which replenishes the consumed on-surface oxygen during the reaction. It was found that the reaction with CO proceeds in two stages. In the first (slow) stage, on-surface oxygen atoms removed by the reaction are immediately replenished by subsurface oxgygen; the second (fast) stage occurs when the subsurface oxygen has been completely consumed and only the reaction of on-surfaces oxygen with CO takes place [Pr87]. Bootsma et al. investigated the CO oxidation on Ag(110) with ellipsometry and found an apparent activation energy of 2.5 kJ/mol at high and -8.8 kJ/mol at low oxygen overages. Bowker et al. found on the same surface an apparent activation energy of -4.8 kJ/mol. The negative value was interpreted as due to a consecutive reaction consisting of an equilibrium between gaseous and adsorbed CO and the oxidation reaction on the surface. With an estimated CO binding energy of 27 kJ/mol, a reaction activation energy of 22 kJ/mol was evaluated.

	$(E_r-E_{des,CO})$ in kJ/mol	E_r in kJ/mol	Reference
Cu(100)	125	-	[Er67]
Cu(110)	21	-	[Er67]
Cu(110)	26	79	[Ha79b]
Cu(110)	25	80	[Ha79c]
Cu(111)	33	75-84	[Ha79a, Ho77]
Ag(110)	2.5 (high Θ_O)	-	[Bo79]
	-8.8 (low Θ_O)	-	
Ag(110)	-4.8 (low Θ_O)	≈ 22	[Bo80]
Au(110)	8	(< 33)	[Ou87a]
Au(110)	-1.8	57	this work
gas phase	-	9-17	[Ko72]
gas phase	-	15	[Cl62]

Table 11.1: Activation energies for the CO oxidation on selected oxidized coinage-metal surfaces.

Outka et al. [Ou87a] reported an apparent activation energy of (8 ± 4) kJ/mol for the CO oxidation on an oxidized Au(110)-(1×2) surface, a result which disagrees with our value of (-1.8 ± 0.9) kJ/mol. A possible explanation for this deviation is given by the different methods for producing chemisorbed oxygen. Outka et al. employed thermal predissociation of O_2 on a hot Pt wire in front of the sample. It cannot be excluded that a different oxygen species than with our method is generated in this way. Furthermore, impurities, especially Pt from the hot wire, may influence the reactivity of the chemisorbed oxygen (although Outka et al. found with AES no Pt contamination).

The data in Table 11.1 indicate that copper has the largest apparent and true activation energies. Silver and gold are comparable in the apparent, but deviate in the true activation energy because of the stronger CO-Au bond (see Chapter 8). Further comparison of E_r reveals similar values for Cu and Au. The value on Ag is much lower and actually close to the gas phase value of 15 kJ/mol, which can be regarded as the lower limit for any surface-mediated CO oxidation reaction.